3D Coordinated Path Following with Disturbance Rejection for Formations of Under-actuated Agents

D.J.W. Belleter and K.Y. Pettersen

Abstract— **In this paper coordinated path following for formations of under-actuated agents in three dimensional space is considered. The agents are controlled to follow a straight-line path whilst being affected by an unknown environmental disturbance. The problem is solved using a twofold approach. In particular, the agents are controlled to the desired path using a guidance law that rejects an unknown, but constant, disturbance. Simultaneously each agent utilises a decentralised nonlinear coordination law to achieve the desired formation. The closed-loop system of path-following and coordination dynamics is analysed using theory for feedback-interconnected systems. In particular, a technique from [1] is used that allows us to analyse a feedback-interconnected systems as a cascaded system. The origin of the closed-loop error dynamics is shown to be globally asymptotically stable. A case study with simulation results is presented to validate the control strategy.**

I. Introduction

In this paper the coordinated path following problem for multi-agent systems with under-actuated agents moving in three dimensional space whilst being affected by an unknown environmental disturbance is considered. Multi-agent systems have attracted a lot of attention from the research community, see for instance [2]–[4] and the references therein. Multi-agent systems can offer several advantages over operations with single robot systems. They can cover a larger area, which is particularly useful in spatially distributed tasks, and which can save time and thus costs. Moreover, they can take over tasks of more complex and costly single robots and can introduce some redundancy for operations in harsh environments.

A lot of the research effort within multi-agent systems has been concentrated on solving the consensus problem, see for instance the seminal work [5], and the flocking/rendezvous problem. The coordinated path-following problem for under-actuated robotic systems, with or without disturbances, has received significantly less attention while it is a problem often occurring in practice. Examples of works that have focused on this problem include [6]–[8] for aircraft and spacecraft, [9]-[10] for land robots, and [11]–[13] for marine vehicles. A framework for information sharing is presented in [6] that is illustrated with an example for space craft. Coordinated control for aerial vehicles is considered in [7], [8], [10] for the disturbance-less case and for kinematic models. Collision avoidance and time constraints are considered in [7] and both [7] and [8] allow for non-straight-line paths. In [9], [11]–[13] dynamic models are considered, however disturbances are not considered in these works. Time delays and communication losses are considered in [11], and [9] combines formation control with an estimator for unknown velocities. The focus of this presented here is on solving the coordinated path following problem in a framework that takes into account the dynamic model of an under-actuated vehicle and an environmental disturbance affecting the vehicle, which is a combination of properties not investigated in the above literature. However, the control strategy is limited to straight-line path following and constant disturbances and does not consider communication losses or time delays as [11].

In particular, this paper aims to extend the framework developed in [14] and [15] to motion in three dimensional space. This requires rejection of a three dimensional environmental disturbance using integral LOS [16]. The three dimensional guidance is combined with a three dimensional extension of the two dimensional coordination control strategy developed in [13] that was extended to include disturbance rejection in [14] and [15]. The derivation of the formation dynamics for the three dimensional case, which now depend on both a horizontal and vertical guidance subsystem, and the subsequent analysis of the new closed-loop system is the main contribution of the paper.

Each vehicle is guided to a desired straight-line path using integral LOS guidance [17]. The path-following error dynamics can then be placed in cascade with the coordination error dynamics that are used to achieve the formation. However, the combination of the adaptive properties of the integral LOS guidance together with the coordination controller creates a feedback in the cascade formed by the full closed-loop dynamics. Therefore classical cascaded systems theory cannot be applied and it is necessary to 'break the loop' [1]. Using this technique we prove that the origin of the full closed-loop error dynamics is uniformly globally asymptotically stable (UGAS).

The paper is organised as follows. The model for the agents and the communication topology are presented in Section II. The controllers and guidance scheme are given in Section III. The closed-loop system is derived in Section IV and stability of the closed-loop system is shown in Section V. Section VI presents the results of a case study. Section VII presents the conclusions.

II. The Agents

This section describes the model of the agents and the environmental disturbance, the control objectives, and the communication topology for the network of agents. To describe the motion of the agents a five degrees of freedom (DOF) manoeuvring model is chosen, which describes an autonomous underwater vehicle (AUV). Therefore the unknown environmental disturbance is modelled as a three dimensional ocean current in this work. The framework developed in this work can be expanded to other systems by choice of a suitable dynamic model, disturbance, and control strategy for that type of system.

A. AUV Model

The model considered in this work is a 5-DOF model for an AUV which describes the motion of the AUV in surge, sway, heave, pitch and yaw. The state of the vehicle $\boldsymbol{\eta} \triangleq [x, y, z, \theta, \psi]^T$ w.r.t. the inertial frame i is expressed in three spatial coordinates x, y, and z and two angles θ and ψ which are the pitch and yaw angle respectively.

This work was partly supported by the Research Council of Norway through its Centres of Excellence funding scheme, project No. 223254 AMOS.

D.J.W. Belleter and K.Y. Pettersen are with the Centre for Autonomous Marine Operations and Systems (AMOS), Department of Engineering Cybernetics, Norwegian University of Science and Technology, NO7491 Trondheim, Norway {dennis.belleter,kristin.y.pettersen}@itk.ntnu.no.

Assumption 1: The roll motion is assumed to be passively stabilised by fins or by gravity and can therefore be neglected when modelling the vessel.

The vector of linear and angular velocities of the vehicle $\boldsymbol{\nu} \triangleq [u, v, w, q, r]^T$ is expressed in a body-fixed frame b and contains the surge velocity u, the sway velocity v, the heave velocity w, the pitch rate q, and the yaw rate r. The vehicles are affected by an ocean current satisfying the following assumption

Assumption 2: The ocean current, $\boldsymbol{V}_c \triangleq [V_x, V_y, V_z]^T$, expressed in the inertial frame i, is assumed to be constant, irrotational and upper-bounded, i.e. $\exists V_{\max} > 0$ such that $\|\boldsymbol{V}_c\| = \sqrt{V_x^2 + V_y^2 + V_z^2} \leq V_{\max}$.

The ocean current velocities in the body-fixed frame b are given by $\boldsymbol{\nu}_c \triangleq [u_c, v_c, w_c, 0, 0]^T$, and are obtained from $[u_c, v_c, w_c]^T = \boldsymbol{R}^T(\theta, \psi)\boldsymbol{V}_c$ where $\boldsymbol{R}(\theta, \psi)$ is the rotation matrix from b to i defined as

$$\boldsymbol{R}(\theta, \psi) \triangleq \begin{bmatrix} \cos(\psi)\cos(\theta) & -\sin(\psi) & \cos(\psi)\sin(\theta) \\ \sin(\psi)\cos(\theta) & \cos(\psi) & \sin(\psi)\sin(\theta) \\ -\sin(\theta) & 0 & \cos(\theta) \end{bmatrix} \tag{1}$$

Using the ocean current velocity we can define the relative velocity in the body-fixed frame as $\boldsymbol{\nu}_r \triangleq \boldsymbol{\nu} - \boldsymbol{\nu}_c = [u_r, v_r, w_r, q, r]^T$ [18]. It is shown in [18] that if the current satisfies Assumption 2 an underwater vehicle can be described using the 5-DOF manoeuvring model:

$$\begin{aligned} \dot{\boldsymbol{\eta}} &= \boldsymbol{J}(\boldsymbol{\eta})\boldsymbol{\nu}_r + [V_x, V_y, V_z, 0, 0]^T, \\ \boldsymbol{M}\dot{\boldsymbol{\nu}}_r + \boldsymbol{C}(\boldsymbol{\nu}_r)\boldsymbol{\nu}_r + \boldsymbol{D}\boldsymbol{\nu}_r + \boldsymbol{g}(\boldsymbol{\eta}) &= \boldsymbol{B}\boldsymbol{f} \end{aligned} \tag{2}$$

The matrix $\boldsymbol{J}(\eta)$ is the velocity transformation matrix defined as $\boldsymbol{J}(\eta) \triangleq \text{bdiag}(\boldsymbol{R}(\theta, \psi), \boldsymbol{T}(\theta))$, with $\boldsymbol{T}(\theta) \triangleq \text{diag}(1, 1/\cos(\theta))$, $|\theta| \neq \pm\pi/2$. The matrix $\boldsymbol{M} = \boldsymbol{M}^T > 0$ is the mass and inertia matrix, matrix $\boldsymbol{D} > 0$ is the hydrodynamic damping matrix, and $\boldsymbol{B}$ is the actuator configuration matrix. The matrix $\boldsymbol{C}$ is the coriolis and centripetal matrix and can be derived from $\boldsymbol{M}$ (see [18]). The gravity vector in CG is given as $\boldsymbol{g}(\boldsymbol{\eta}) \triangleq [0, 0, 0, BG_z W \sin(\theta), 0]^T$, with BG_z the vertical distance between CG and CB, and W is the weight of the vehicle. The control input vector $\boldsymbol{f}$ is defined as $\boldsymbol{f} \triangleq [T_u, T_q, T_r]^T$ and contains the surge thrust T_u, the pitch rudder angle T_q, and the yaw rudder angle T_r.

Assumption 3: The vehicles are neutrally buoyant and the center of gravity (CG) and the center of buoyancy (CB) are located along the same vertical axis in the body-fixed frame.

Assumption 4: The vehicles are assumed to be xz plane symmetric and have a large length to width ratio.

Assumption 5: The surge mode is decoupled from the other degrees of freedom and consider only the dominating interconnections, i.e. the interconnections between sway and yaw and between heave and pitch.

Assumption 6: Damping is considered linear.

Remark 1: Assumptions 1 and 3-6 are common assumptions in manoeuvring control of slender-body AUVs [18].

Considering Assumptions 3-6 matrices $\boldsymbol{M}$, $\boldsymbol{D}$, and $\boldsymbol{B}$ have the following structure

$$\boldsymbol{M} \triangleq \begin{bmatrix} m_{11} & 0 & 0 & 0 & 0 \\ 0 & m_{22} & 0 & 0 & m_{25} \\ 0 & 0 & m_{33} & m_{34} & 0 \\ 0 & 0 & m_{43} & m_{44} & 0 \\ 0 & m_{52} & 0 & 0 & m_{55} \end{bmatrix}, \tag{3}$$

$$\boldsymbol{D} \triangleq \begin{bmatrix} d_{11} & 0 & 0 & 0 & 0 \\ 0 & d_{22} & 0 & 0 & d_{25} \\ 0 & 0 & d_{33} & d_{34} & 0 \\ 0 & 0 & d_{43} & d_{44} & 0 \\ 0 & d_{52} & 0 & 0 & d_{55} \end{bmatrix}, \quad \boldsymbol{B} \triangleq \begin{bmatrix} b_{11} & 0 & 0 \\ 0 & 0 & b_{23} \\ 0 & b_{32} & 0 \\ 0 & b_{42} & 0 \\ 0 & 0 & b_{53} \end{bmatrix}. \tag{4}$$

The location of the body-fixed frame is chosen to be at $(x_g^*, 0, 0)$ such that $\boldsymbol{M}^{-1}\boldsymbol{B}\boldsymbol{f} = [\tau_u, 0, 0, \tau_q, \tau_r]^T$. Note that the model is under-actuated in sway and heave. The point $(x_g^*, 0, 0)$ always exists for AUVs of cylindrical shape employing symmetric steering and diving control surfaces [19] and the body-fixed frame can always be translated to this location [18].

The model can be expanded into component form as

$$\begin{aligned} \dot{x} &= u_r\cos(\psi)\cos(\theta) - v_r\sin(\psi) \\ &\quad + w_r\cos(\psi)\sin(\theta) + V_x \end{aligned} \tag{5a}$$

$$\begin{aligned} \dot{y} &= u_r\sin(\psi)\cos(\theta) + v_r\cos(\psi) \\ &\quad + w_r\sin(\psi)\sin(\theta) + V_y \end{aligned} \tag{5b}$$

$$\dot{z} = -u_r\sin(\theta) + w_r\cos(\theta) + V_z \tag{5c}$$

$$\dot{\theta} = q \tag{5d}$$

$$\dot{\psi} = r/\cos(\theta) \tag{5e}$$

$$\dot{u}_r = F_{u_r}(v_r, w_r, q, r) - (d_{11}/m_{11})u_r + \tau_u \tag{5f}$$

$$\dot{v}_r = X_{v_r}(u_r)q + Y_{v_r}(u_r)v_r \tag{5g}$$

$$\dot{w}_r = X_{w_r}(u_r)q + Y_{w_r}(u_r)w_r + Z_{w_r}\sin(\theta) \tag{5h}$$

$$\dot{q} = F_q(\theta, u_r, w_r, q) + \tau_q \tag{5i}$$

$$\dot{r} = F_r(u_r, v_r, r) + \tau_r \tag{5j}$$

The definitions of F_{u_r}, X_{v_r}, Y_{v_r}, X_{w_r}, Y_{w_r}, Z_{w_r}, F_q, and F_r are given in Appendix I.

Assumption 7: The functions $Y_{v_r}(u_r)$ and $Y_{w_r}(u_r)$ satisfy

$$\begin{aligned} Y_{v_r}(u_r) &\leq -Y_{v_r}^{\min} < 0, \, \forall u_r \in [-V_{\max}, U_{rd} + a], \\ Y_{w_r}(u_r) &\leq -Y_{w_r}^{\min} < 0, \, \forall u_r \in [-V_{\max}, U_{rd} + a], \end{aligned}$$

where a is a parameter of the formation control law to be defined later, $V_{\max}$ the bound on the current from Assumption 2, and U_{rd} the desired relative surge velocity.

Remark 2: Assumption 7 is satisfied for commercial vessels by design, since the converse would imply an undamped or nominally unstable vessel in sway and heave.

B. The Control Objectives

The goal is coordinating the motion of n AUVs along a straight-line path $\mathcal{P}$ in 3D space to achieve a given formation. Without loss of generality the inertial frame is chosen such that its x-axis is aligned with the desired path, and consequently $\mathcal{P} \triangleq \{(x, y, z) \in \mathbb{R}^3 : y, z = 0\}$. For the jth AUV in the formation the goal can be characterised by the following control objectives

$$\lim_{t\to\infty} y_j(t) - D_{yj} = 0, \tag{6a}$$

$$\lim_{t\to\infty} z_j(t) - D_{zj} = 0, \tag{6b}$$

$$\lim_{t\to\infty} \psi_j(t) = \psi_{ss}, \quad \psi_{ss} \in (-\tfrac{\pi}{2}, \tfrac{\pi}{2}), \tag{6c}$$

$$\lim_{t\to\infty} \theta_j(t) = \theta_{ss}, \quad \theta_{ss} \in (-\tfrac{\pi}{2}, \tfrac{\pi}{2}), \tag{6d}$$

$$\lim_{t\to\infty} u_{r_j}(t) - U_{rd} = 0, \tag{6e}$$

$$\lim_{t\to\infty} x_j(t) - x_i(t) - d_{ji} = 0. \tag{6f}$$

Control objectives (6a) and (6b) express the path-following control objectives, where D_{yj} and D_{zj} are offsets to the path $\mathcal{P}$ that are given by the desired formation structure. Control objectives (6c) and (6d) describe the desired side-slipping motion in steady-state, which is necessary for disturbance rejection in the transversal direction of the path despite the absence of actuation in sway and heave. Control objective (6e) assures that all vehicles achieve the same desired velocity. Control objective (6f) specifies that the inter vehicle distance along the path should converge to a pre-defined value d_{ji} given by the desired formation structure.

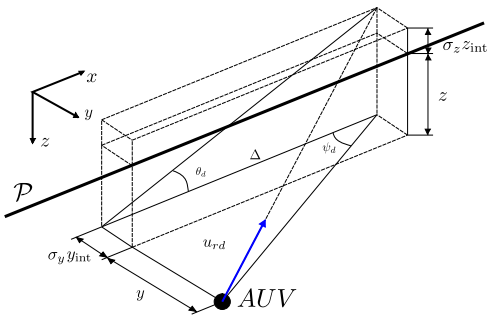

Fig. 1. Geometry of the 3D-ILOS path-following for $\Delta_y = \Delta_z = \Delta$

C. Communication Topology

To synchronise the along-path distance, communication of the along-path distance between the vehicles is required. This information can then be used in local synchronisation laws resulting in a decentralised approach. Graph theory [20] is used to model the communication.

The communication network is represented by a directed graph or digraph $\mathcal{G}(V, E)$, where V is a set of vertices representing the vessels and E is a set of edges representing the communication flow. The neighbourhood $\mathcal{A}_j$ of v_j is the set of vertices $v_i \in V$ such that there is an edge from v_j to v_i. Hence, when controlling vessel j only the along-path position x_i of the vessels where $i \in \mathcal{A}_j$ may be used. The above allows us to give some definitions, based on [21], that are used in the analysis of the formation dynamics. A vertex $v_k \in V$ reachable from vertex $v_i \in V$ if there is a path from v_i to v_k. A vertex is globally reachable if it can be reached from every vertex in $\mathcal{G}(V, E)$. The graph is said to be strongly connected, if all vertices of $\mathcal{G}(V, E)$ are globally reachable.

III. Control System

In this section the control system is proposed. In the first subsection the path-following control strategy is introduced. The second subsection describes the controller used to achieve along-path coordination.

A. Path-Following Control

Path-following is achieved using integral line-of-sight (LOS) guidance combined with feedback linearising controllers for the yaw and pitch angle (see Fig. 1).

1) Yaw Control: The desired yaw angle is calculated using an integral LOS guidance law, first introduced in [22], based on the y distance to the path which results in

$$\psi_d \triangleq -\tan^{-1}\left(\frac{(y-D_{yj})+\sigma_y y_{\text{int}}}{\Delta_y}\right), \quad \Delta_y > 0, \tag{7a}$$

$$\dot{y}_{\text{int}} = \frac{\Delta_y (y-D_{yj})}{((y-D_{yj})+\sigma_y y_{\text{int}})^2+\Delta_y^2}, \tag{7b}$$

with $\sigma_y > 0$ the integral gain and Δ_y the look-ahead distance. The desired yaw angle is tracked using the following feedback linearising yaw rate controller

$$\begin{aligned}\tau_r = &- F_r(u_r, v_r, r) - q\sin(\theta)\dot{\psi} \\ &+ \cos(\theta)\left[\ddot{\psi}_d - k_\psi(\psi-\psi_d) - k_r(\dot{\psi}-\dot{\psi}_d)\right],\end{aligned} \tag{8}$$

with $k_\psi > 0$ and $k_r > 0$ the proportional and derivative controller gains respectively.

2) Pitch Control: The desired pitch angle is calculated using an integral LOS guidance based on the z distance to the path, resulting in

$$\theta_d \triangleq \tan^{-1}\left(\frac{(z-D_{zj})+\sigma_z z_{\text{int}}}{\Delta_z}\right), \quad \Delta_z > 0, \tag{9a}$$

$$\dot{z}_{\text{int}} = \frac{\Delta_z (z-D_{zj})}{((z-D_{zj})+\sigma_z z_{\text{int}})^2+\Delta_z^2}, \tag{9b}$$

with $\sigma_z > 0$ the integral gain and Δ_z the look-ahead distance. The desired pitch angle is tracked using the following feedback linearising pitch rate controller

$$\tau_q = -F_q(\theta, u_r, w_r, q) + \ddot{\theta}_d - k_\theta(\theta-\theta_d) - k_q(\dot{\theta}-\dot{\theta}_d), \tag{10}$$

with $k_\theta > 0$ and $k_q > 0$ the proportional and derivative controller gains respectively.

B. Coordination Control

The coordination controller consists of a velocity assignment proportional to the coordination error combined with a feedback linearising surge controller. The velocity assignment is chosen as

$$u_{c_j} \triangleq U_{rd} - g\Big(\sum_{i\in\mathcal{A}_j}(x_j - x_i - d_{ji})\Big), \tag{11}$$

with U_{rd} the desired constant relative surge velocity and $g(x)$ proportional to the along-path coordination error. The function $g(x) : \mathbb{R} \to \mathbb{R}$ should be a continuously differentiable saturation-like function satisfying

$$\begin{aligned} -a \le g(x) \le a, \quad \forall x \in \mathbb{R}, \quad g(0) = 0, \\ 0 < g'(x) \le \mu, \quad \forall x \in \mathbb{R}, \quad g'(x) \triangleq dg/dx \end{aligned} \tag{12}$$

where a is the parameter from Assumption 7, and $\mu > 0$ is an arbitrary constant. This also implies that the function $g(x)$ should be a sector function belonging to the sector $[0, \mu]$. A suitable choice for $g(x)$ is for example

$$g(x) \triangleq \tfrac{2a}{\pi}\tan^{-1}(x). \tag{13}$$

Assumption 8: The desired relative surge velocity u_c satisfies the following condition:

$$u_c > \max\left\{V_{\max} + \tfrac{5}{2}\left|\frac{Z_{w_r}}{Y_{w_r}(u_c)}\right|, 2V_{\max} + 2\left|\frac{Z_{w_r}}{Y_{w_r}(u_c)}\right|\right\}$$

and consequently $U_{rd} > u_c + a$ to allow for the necessary velocity manipulation by the coordination law.

To track u_{c_j} the following feedback linearising P controller is applied to each vessel

$$\tau_u = -F_{u_r}(v_r, r) + \tfrac{d_{11}}{m_{11}}u_{c_j} + \dot{u}_{c_j} - k_{u_r}(u_r - u_{c_j}), \tag{14}$$

with $k_{u_r} > 0$ a constant gain. Note that part of the surge damping is not cancelled to guarantee some robustness w.r.t. model uncertainties.

Using the notation

$$X_\alpha^{\max_j} \triangleq \max_{u_{c_j}\in[U_{\min}, U_{\max}]} |X_{\alpha,j}(u_{c_j})| \tag{15}$$

$$Y_\alpha^{\min_j} \triangleq \min_{u_{c_j}\in[U_{\min}, U_{\max}]} |Y_{\alpha,j}(u_{c_j})| \tag{16}$$

with $\alpha \in \{v_r, w_r\}$, $U_{\min} = U_{rd} - a$, and $U_{\max} = U_{rd} + a$ where the main result can then be formulated as follows.

Theorem 1: Consider a formation of n vessels described by (5). Suppose that u_d is continuously differentiable, Assumptions 2-8 are satisfied, and the communication graph contains at least one globally reachable vertex. If the look-ahead distances Δ_y and Δ_z, and the integral gains σ_y and σ_z satisfy the conditions

$$\Delta_y = \frac{|X_{v_r}^{\max}|}{|Y_{v_r}^{\min}|}\left[\tfrac{5}{4}\tfrac{\Gamma_{\max}+V_{\max}+\sigma_y}{\Gamma_{\min}-V_{\max}-\sigma_y}+1\right], \tag{17a}$$

$$\Delta_z = \frac{|X_{w_r}^{\max}|}{|Y_{w_r}^{\min}|}\rho(\sigma_z)\left[\tfrac{5}{4}\tfrac{\Gamma_{\max}+V_{\max}+\sigma_z}{\Gamma_{\min}-V_{\max}-\sigma_z}+1\right], \tag{17b}$$

$$0 < \sigma_y < \Gamma_{\inf} - V_{\max}, \tag{17c}$$

$$0 < \sigma_z < U_{\min} - V_{\max} - \frac{5}{2}\left|\frac{Z_{w_r}}{Y^{\min}_{w_r}}\right|, \tag{17d}$$

$$\text{with} \qquad \rho(\sigma_z) \triangleq \frac{U_{\max} - V_{\max} - \sigma_z}{U_{\min} - V_{\max} - \sigma_z - \frac{5}{2}\left|\frac{Z_{w_r}}{Y^{\min}_{w_r}}\right|} \tag{17e}$$

for $j = 1, \ldots, n$, then the controllers (7-10), (14) guarantee achievement of the control goals (6) with $\psi_{ss} = -\tan^{-1}(V_y/\sqrt{\Gamma(s)^2 - V_y^2})$ and $\theta_{ss} = \tan^{-1}(s)$.

Remark 3: The constant s and the function $\Gamma(s)$ are defined in the next section when the closed-loop dynamics are derived.
The proof of Theorem 1 is given in Section V which considers the closed-loop stability of the error dynamics.

IV. Closed-loop System

In this section the closed-loop dynamics are formulated. The closed-loop path-following error and tracking error dynamics are derived first. The coordination error dynamics are derived second and finally the full closed-loop system is presented.

A. Path-following and Tracking Error Dynamics

In this subsection the tracking and path-following error dynamics are considered. The derivation of these dynamics follow those in [16] and [17], in which the same path-following dynamics are investigated for single vehicles. The tracking errors are analysed by substituting the controllers (8), (10), and (14) into the dynamical system (5). For analysis we introduce the vector $\boldsymbol{\xi} \triangleq [\tilde{u}_r, \tilde{\psi}, \tilde{r}, \tilde{\theta}, \tilde{q}]^T$, with tracking errors $\tilde{u}_r \triangleq u_r - u_c$, $\tilde{\psi} \triangleq \psi - \psi_d$, $\tilde{r} \triangleq r - \dot{\psi}_d$, $\tilde{\theta} \triangleq \theta - \theta_d$, and $\tilde{q} \triangleq q - \dot{\theta}_d$. The tracking error dynamics are given by

$$\dot{\boldsymbol{\xi}} = \begin{bmatrix} -k_{u_r} - \frac{d_{11}}{m_{11}} & 0 & 0 & 0 & 0 \\ 0 & 0 & 1 & 0 & 0 \\ 0 & -k_\psi & -k_r & 0 & 0 \\ 0 & 0 & 0 & 0 & 1 \\ 0 & 0 & 0 & -k_\theta & -k_q \end{bmatrix} \boldsymbol{\xi} \triangleq \Sigma \boldsymbol{\xi}. \tag{18}$$

The system (18) is linear and time-invariant and k_{u_r}, d_{11}/m_{11}, k_ψ, k_θ, k_q, and k_r are all strictly positive. Therefore, Σ is Hurwitz and the origin of the tracking error dynamics (18) is uniformly globally exponentially stable (UGES).

The first part of the path-following dynamics consists of the $z - w_r$ subsystem given by

$$\dot{z}_{\text{int}} = \frac{\Delta_z (z - D_{zj})}{((z - D_{zj}) + \sigma_z z_{\text{int}})^2 + \Delta_z^2}, \tag{19a}$$

$$\dot{z} = -u_r \sin(\tilde{\theta} + \theta_d) + w_r \cos(\tilde{\theta} + \theta_d) + V_z, \tag{19b}$$

$$\dot{w}_r = X_{w_r}(u_r) q + Y_{w_r}(u_r) w_r + Z_{w_r} \sin(\tilde{\theta} + \theta_d). \tag{19c}$$

In [17] it is shown that the equilibrium of (19) satisfies

$$z^{\text{eq}} = D_{zj}, \quad w_r^{\text{eq}} = u_c \frac{\sigma_z z_{\text{int}}^{\text{eq}}}{\Delta_z} - V_z \sqrt{\left(\frac{\sigma_z z_{\text{int}}^{\text{eq}}}{\Delta_z}\right)^2 + 1}$$

where $z_{\text{int}}^{\text{eq}}$ is the unique solution of:

$$s\sqrt{s^2 + 1} = \frac{V_z}{u_c} s^2 - \frac{Z_{w_r}}{u_c Y^{u_c}_{w_r}} s + \frac{V_z}{u_c} \tag{20}$$

with $s \triangleq \sigma_z z_{\text{int}}^{\text{eq}} / \Delta_z$.

The second part of the path-following dynamics is formed by the $y - v_r$ subsystem given by

$$\dot{y}_{\text{int}} = \frac{\Delta_y (y - D_{yj})}{((y - D_{yj}) + \sigma_y y_{\text{int}})^2 + \Delta_y^2}, \tag{21a}$$

$$\dot{y} = u_r \sin(\tilde{\psi} + \psi_d) \cos(\tilde{\theta} + \theta_d) + v_r \cos(\tilde{\psi} + \psi_d) + w_r \sin(\tilde{\psi} + \psi_d) \sin(\tilde{\theta} + \theta_d) + V_y, \tag{21b}$$

$$\dot{v}_r = X_{v_r}(u_r)(\dot{\tilde{\psi}} + \dot{\psi}_d) \cos(\tilde{\theta} + \theta_d) + Y_{v_r}(u_r) v_r, \tag{21c}$$

for which it is shown in [17] that the equilibrium is given by

$$y_{\text{int}}^{\text{eq}} = \frac{\Delta_y}{\sigma_y} \frac{V_y}{\sqrt{\Gamma(s)^2 - V_y^2}}, \quad y^{\text{eq}} = D_{yj}, \quad v_r^{\text{eq}} = 0,$$
$$\text{where} \quad \Gamma(s) \triangleq u_c \frac{1}{\sqrt{s^2+1}} - \frac{Z_{w_r}}{Y^{u_c}_{w_r}} \frac{s^2}{s^2+1}.$$

The equilibrium point of the (19) and (21) can be moved to the origin using the introduction of the following error variables

$$e_{z_1} \triangleq z_{\text{int}} - z_{\text{int}}^{\text{eq}},\ e_{z_2} \triangleq (z - D_{zj}) - \sigma_z e_{z_1},\ e_{z_3} \triangleq w_r - w_{\text{int}}^{\text{eq}}$$
$$e_{y_1} \triangleq y_{\text{int}} - y_{\text{int}}^{\text{eq}}, \quad e_{y_2} \triangleq (y - D_{yj}) - \sigma_y e_{y_1},$$

and including the tracking error dynamics (18), the system can be written in the cascaded form

$$\begin{bmatrix} \dot{e}_{y_1} \\ \dot{e}_{y_2} \\ \dot{v}_r \end{bmatrix} = \boldsymbol{A}_2(e_{y_2}) \begin{bmatrix} e_{y_1} \\ e_{y_2} \\ v_r \end{bmatrix} + \boldsymbol{B}_2(e_{y_2}) p(e_{y_2}) + \boldsymbol{H}_2 \boldsymbol{\chi},$$
$$\dot{\boldsymbol{\chi}} = \begin{bmatrix} \boldsymbol{A}_1(e_{z_2}) & \boldsymbol{H}_1 \\ \boldsymbol{0} & \Sigma \end{bmatrix} \boldsymbol{\chi} + \begin{bmatrix} \boldsymbol{B}_1(e_{z_2}) \\ \boldsymbol{0} \end{bmatrix} f(e_{z_2}) \tag{22}$$

with $\boldsymbol{\chi} \triangleq [e_{z_1}, e_{z_2}, e_{z_3}, \boldsymbol{\xi}^T]^T$. Hence, the tracking errors are placed in cascade with the $z - w_r$ subsystem and this cascade is placed in cascade with the $y - v_r$ subsystem. The matrices $\boldsymbol{A}_1(e_{z_2})$ and $\boldsymbol{A}_2(e_{y_2})$ can be found in (29) and (30), matrices $\boldsymbol{B}_1(e_{z_2})$, $\boldsymbol{B}_2(e_{y_2})$, $f(e_{z_2})$, and $p(e_{y_2})$ are defined as

$$\boldsymbol{B}_1 \triangleq \left[0, V_z, \frac{\Delta_z^2 X^{u_c}_{w_r} V_z}{(e_{z_2} + \sigma_z z_{\text{int}}^{\text{eq}})^2 + \Delta_z^2} - Z_{w_r} \frac{s}{\sqrt{s^2+1}}\right]^T \tag{23}$$

$$\boldsymbol{B}_2 \triangleq \left[0, V_y, \frac{-\Delta_y^2 X^{u_c}_{v_r} V_y}{\sqrt{s^2+1}(e_{y_2} + \sigma_y y_{\text{int}}^{\text{eq}})^2 + \Delta_y^2}\right]^T \tag{24}$$

$$f(e_{z_2}) = 1 - \frac{\sqrt{(\sigma_z z_{\text{int}}^{\text{eq}})^2 + \Delta_z^2}}{\sqrt{(e_{z_2} + \sigma_z z_{\text{int}}^{\text{eq}})^2 + \Delta_z^2}} \tag{25}$$

$$p(e_{y_2}) = 1 - \frac{\sqrt{(\sigma_y y_{\text{int}}^{\text{eq}})^2 + \Delta_y^2}}{\sqrt{(e_{y_2} + \sigma_y y_{\text{int}}^{\text{eq}})^2 + \Delta_y^2}}. \tag{26}$$

The interconnection matrices $\boldsymbol{H}_1(z, z_{\text{int}}, \theta_d, w_r, \boldsymbol{\zeta})$ and $\boldsymbol{H_2}(y, y_{\text{int}}, \theta_d, \psi_d, v_r, \boldsymbol{\chi})$ contain the terms perturbing terms for the cascade from control tracking errors to the $z - w_r$ subsystem and the perturbing terms van $z - w_r$ to the $y - v_r$ subsystem respectively. The interconnection term $\boldsymbol{H}_1 \boldsymbol{\xi}$ goes to zero when $\boldsymbol{\xi}$ goes to zero and $\boldsymbol{H_2} \boldsymbol{\chi}$ goes to zero when $\boldsymbol{\chi}$ goes to zero. The interconnection matrices are given by

$$\boldsymbol{H}_1 \triangleq \begin{bmatrix} 0 & 0 \\ 1 & 0 \\ \frac{\Delta_z X_{w_r}(\tilde{u}_r + u_c)}{(e_{z_2} + \sigma_z z_{\text{int}}^{\text{eq}})^2 + \Delta_z^2} & 1 \end{bmatrix} \begin{bmatrix} \boldsymbol{h}_z^T \\ \boldsymbol{h}_{w_r}^T \end{bmatrix} \tag{27}$$

$$\boldsymbol{H}_2 \triangleq \begin{bmatrix} 0 & 0 \\ 1 & 0 \\ -\frac{\Delta_y X_{v_r}(\tilde{u}_r + u_c)\cos(\tilde{\theta} + \theta_d)}{(e_{y_2} + \sigma_y y_{\text{int}}^{\text{eq}})^2 + \Delta_y^2} & 1 \end{bmatrix} \begin{bmatrix} \boldsymbol{h}_y^T \\ \boldsymbol{h}_{v_r}^T \end{bmatrix} \tag{28}$$

where the expressions for $\boldsymbol{h}_z^T$, $\boldsymbol{h}_{w_r}^T$, $\boldsymbol{h}_y^T$, and $\boldsymbol{h}_{v_r}^T$ can be found in Appendix I.

In [17] it is shown that the path-following cascaded system (22) has a UGAS equilibrium at the origin for a constant velocity satisfying Assumption 8 and constants satisfying (17).

Remark 4: Note that for the case of a constant velocity u_c we have $U_{\max} \equiv U_{\min} \equiv u_c$, $X^{\max} \equiv X^{\min} \equiv X^{u_c}$, and $Y^{\max} \equiv Y^{\min} \equiv Y^{u_c}$ for the constants in (17).

Remark 5: Note that the proof in [17] applies only for a constant velocity u_c. However in the case considered here the velocity is not constant, and therefore the proof cannot be directly applied to the coordinated path-following scenario. However it will be shown that when analysing the closed-loop in Section V we can still utilise

this proof when the velocity satisfies $u_c \in [U_{rd} - a, U_{rd} + a]$ as defined in (11).

Remark 6: Despite the singularity in θ in the open loop system (2), this singularity does not appear in the closed-loop path-following error dynamics (22). Therefore, global results can be achieved for the path-following error. However, for the AUV model $\theta_0 = \pm\pi/2$ should be excluded as an initial condition.

B. Coordination Error Dynamics

The coordination error dynamics are expressed in the x-direction of the inertial frame and therefore we consider (5a)

$$\begin{aligned}\dot{x} &= (u_c + \tilde{u}_r)\cos(\tilde{\psi} + \psi_d)\cos(\tilde{\theta} + \theta_d) - v_r \sin(\tilde{\psi} + \psi_d) \\ &\quad + w_r \cos(\tilde{\psi} + \psi_d)\sin(\tilde{\theta} + \theta_d) + V_x \\ &= \Gamma(s)\cos(\psi_d) + g(x)\cos(\psi_{ss})\cos(\theta_{ss}) + V_x + \boldsymbol{h}_x^T \boldsymbol{\zeta}\end{aligned} \tag{31}$$

where $\boldsymbol{h}_x^T \boldsymbol{\zeta}$ is the interconnection term between the coordination error dynamics and path-following error dynamics with $\boldsymbol{\zeta} = [e_{y_1}, e_{y_2}, v_r, \boldsymbol{\chi}]^T$. The elements of $\boldsymbol{h}_x^T$ are given by

$$\begin{aligned}
h_{x1} &= h_{x4} = h_{x9} = h_{x11} = 0 \\
h_{x2} &= g(x)\cos(\theta_{ss})\left[\tfrac{\cos(\psi_t)-1}{e_{y2}}\cos(\psi_{ss}) + \tfrac{\sin(\psi_t)}{e_{y2}}\sin(\psi_{ss})\right] \\
h_{x3} &= -\sin(\tilde{\psi} + \psi_d) \\
h_{x5} &= u_c \cos(\psi_d)\left[\tfrac{\cos(\theta_t)-1}{e_{z2}}\cos(\theta_{ss}) + \tfrac{\sin(\theta_t)}{e_{z2}}\sin(\theta_{ss})\right] \\
&\quad + w_r^{\text{eq}}\cos(\psi_d)\left[\tfrac{\sin(\theta_t)}{e_{z2}}\cos(\theta_{ss}) + \tfrac{\cos(\theta_t)-1}{e_{z2}}\sin(\theta_{ss})\right] \\
h_{x6} &= \cos(\tilde{\psi} + \psi_d)\sin(\tilde{\theta} + \theta_d) \\
h_{x7} &= \cos(\tilde{\psi} + \psi_d)\cos(\tilde{\theta} + \theta_d) \\
h_{x8} &= \left[w_r^{\text{eq}}\sin(\tilde{\theta} + \theta_d) + u_c\cos(\tilde{\theta} + \theta_d)\right] \\
&\quad \left[\tfrac{\cos(\tilde{\psi})-1}{\tilde{\psi}}\cos(\psi_d) - \tfrac{\sin(\tilde{\psi})}{\tilde{\psi}}\sin(\psi_d)\right] \\
h_{x10} &= [w_r^{\text{eq}}\cos(\psi_d) + u_c\cos(\psi_d)] \\
&\quad \left[\tfrac{\sin(\tilde{\theta})}{\tilde{\theta}}\cos(\theta_d) + \tfrac{\cos(\tilde{\theta})-1}{\tilde{\theta}}\sin(\theta_d)\right].
\end{aligned} \tag{32}$$

Using that the steady-state path-following velocity U_x is given by $U_x \triangleq \Gamma(s)\cos(\psi_{ss}) + V_x$, we can introduce the change of coordinates $\vartheta_j \triangleq x_j - d_j - \int_{t_0}^t U_x ds$ for $j = 1, \ldots, n$ where d_j is such that $d_j - d_i = d_{ji}$. The path-following dynamics (31) can be transformed into the coordination error dynamics using this changes of coordinates

$$\dot{\vartheta}_j = -g\Big(\sum_{i \in \mathcal{A}_j}(\vartheta_j - \vartheta_i)\Big)\cos(\psi_{ss})\cos(\theta_{ss}) + \boldsymbol{h}_x^T \boldsymbol{\zeta}. \tag{33}$$

Remark 7: Note that $\vartheta_j - \vartheta_i = 0, \forall i, j = 1, \ldots, n$ implies that (6f) is satisfied and along-path coordination is achieved. Moreover, since $\tilde{u}_r$ converges exponentially to zero satisfaction of (6f) also implies that (6e) is satisfied.

To consider all vessels we write the system in vector form by defining $\boldsymbol{\vartheta} \triangleq [\vartheta_1, \ldots, \vartheta_n]^T$, $\boldsymbol{g}(\boldsymbol{\vartheta}) \triangleq [g(\vartheta_1), \ldots, g(\vartheta_n)]^T$, $\boldsymbol{\Lambda} \triangleq [\mathbf{diag}\{\cos(\psi_{ss_1})\cos(\theta_{ss_1}), \ldots, \cos(\psi_{ss_n})\cos(\theta_{ss_n})\}]$, $\boldsymbol{\zeta} \triangleq [\boldsymbol{\zeta}_1^T, \ldots, \boldsymbol{\zeta}_n^T]^T$, and $\boldsymbol{H}_x \triangleq [\boldsymbol{h}_{x_1}, \ldots, \boldsymbol{h}_{x_n}]^T$, such that (33) can be written as

$$\dot{\boldsymbol{\vartheta}} = -\boldsymbol{\Lambda}\boldsymbol{g}(\boldsymbol{L}\boldsymbol{\vartheta}) + \boldsymbol{H}_x(\boldsymbol{\zeta}, \boldsymbol{\vartheta})\boldsymbol{\zeta} \tag{34}$$

where $\boldsymbol{L}$ is the Laplacian matrix of the graph $\mathcal{G}$ with elements:

$$l_{ji} \triangleq \begin{cases} \delta_j & \text{if } j = i \\ -1, & \text{if } j \neq i \ \wedge \ (j,i) \in E, \ j, i = 1, \ldots, n \\ 0, & \text{otherwise} \end{cases} \tag{35}$$

with δ_j the number of outgoing edges from v_j. By definition the Laplacian has one or more eigenvalues at zero with the vector of all ones as eigenvector. If the graph is strongly connected, i.e. it has n globally reachable vertices, then the zero eigenvalue is simple and $\boldsymbol{L}$ is symmetric and positive semi-definite (see [20], [21]).

As stated in [13] the consensus properties of the coordination-error dynamics cannot be determined by simply analysing its stability properties, since it can have multiple equilibria depending on the network topology. Therefore, a coordinate transform is proposed in [13, Lemma 2] which can also be derived for system equation (34).

Lemma 1 ([13, Lemma 2]): Consider system (34). Under the condition of Theorem 1 there exists a coordinate transformation $\boldsymbol{\phi} \triangleq \boldsymbol{T}\boldsymbol{\vartheta}$, $\boldsymbol{T} \in \mathbb{R}^{(n-1)\times n}$, such that the following holds:

1) $\boldsymbol{\phi} = \mathbf{0}$ implies that $\vartheta_1 = \ldots = \vartheta_n$;
2) the dynamics of $\boldsymbol{\phi}$ are of the form
$$\dot{\boldsymbol{\phi}} = \boldsymbol{f}(\boldsymbol{\phi}) + \boldsymbol{G}(\boldsymbol{\zeta}, \boldsymbol{\phi})\boldsymbol{\zeta} \tag{36}$$
with $\boldsymbol{G}(\boldsymbol{\zeta}, \boldsymbol{\phi})$ globally bounded, uniformly in $\boldsymbol{\zeta}$ and $\boldsymbol{\phi}$;
3) $\dot{\boldsymbol{\phi}} = \boldsymbol{f}(\boldsymbol{\phi})$ is UGAS with positive definite and radially unbounded Lyapunov function $V = V(\boldsymbol{\phi})$ satisfying
$$\frac{\partial V}{\partial \boldsymbol{\phi}}(\boldsymbol{\phi})\boldsymbol{f}(\boldsymbol{\phi}) \leq -W(\boldsymbol{\phi}) < 0, \ \forall \boldsymbol{\phi} \in \mathbb{R}^{n-1} \setminus \{\mathbf{0}\} \tag{37}$$
$$\left\| \frac{\partial V}{\partial \boldsymbol{\phi}}(\boldsymbol{\phi}) \right\| \leq C_1, \ \forall \boldsymbol{\phi} \in \mathbb{R}^{n-1}. \tag{38}$$

Proof: The proof for the case considered here is equivalent to that in [14] and therefore omitted in favour of the resulting transformation. The transformation is based on a partitioning of the Laplacian:

$$\boldsymbol{L} = \begin{bmatrix} \boldsymbol{L}_1 & \boldsymbol{L}_2 \\ \mathbf{0} & \boldsymbol{M}_3\boldsymbol{M}_3^T \end{bmatrix} \tag{39}$$

resulting in the coordinate transformation:

$$\boldsymbol{\phi} \triangleq \begin{bmatrix} \boldsymbol{L}_1 & \boldsymbol{L}_2 \\ \mathbf{0} & \boldsymbol{M}_3^T \end{bmatrix} \boldsymbol{\vartheta} \triangleq \boldsymbol{T}\boldsymbol{\vartheta}. \tag{40}$$

Applying this coordinate transform results in

$$\dot{\boldsymbol{\phi}} = \begin{bmatrix} -\boldsymbol{L}_1\boldsymbol{\Lambda}_1\boldsymbol{g}_1(\boldsymbol{\phi}_1) - \boldsymbol{L}_2\boldsymbol{\Lambda}_2\boldsymbol{g}_2(\boldsymbol{\kappa}) \\ -\boldsymbol{M}_3^T\boldsymbol{\Lambda}_2\boldsymbol{g}_2(\boldsymbol{\kappa}) \end{bmatrix} + \boldsymbol{T}\boldsymbol{H}_x(\boldsymbol{\zeta}, \boldsymbol{\vartheta})\boldsymbol{\zeta} \tag{41}$$
$$\triangleq \boldsymbol{f}(\boldsymbol{\phi}) + \boldsymbol{G}(\boldsymbol{\zeta}, \boldsymbol{\vartheta})\boldsymbol{\zeta} \tag{42}$$

where $\boldsymbol{\phi} = [\boldsymbol{\phi}_1^T, \boldsymbol{\phi}_2^T]^T$, with $\boldsymbol{\phi}_1 \in \mathbb{R}^{n-r}$ and $\phi_2 \in \mathbb{R}^r$, and we defined $\boldsymbol{\kappa} \triangleq \boldsymbol{M}_3\boldsymbol{\phi}_2$ to simplify notation. Moreover, using (32) it is straightforward to verify that $\boldsymbol{G}(\boldsymbol{\zeta}, \boldsymbol{\phi}) \triangleq \boldsymbol{T}\boldsymbol{H}_x(\boldsymbol{\zeta}, \boldsymbol{\phi})$ is globally bounded in its arguments. ∎

The total closed-loop system can now be formulated as:

$$\dot{\boldsymbol{\phi}} = \boldsymbol{f}(\boldsymbol{\phi}) + \boldsymbol{G}(\boldsymbol{\zeta}, \boldsymbol{\phi})\boldsymbol{\zeta} \tag{43a}$$

$$\dot{\boldsymbol{\zeta}} = \left[\begin{array}{c|cc} \boldsymbol{A}_2(e_{y_2}) & \multicolumn{2}{c}{\boldsymbol{H}_2} \\ \hline \mathbf{0} & \boldsymbol{A}_1(e_{z_2}) & \boldsymbol{H}_1 \\ & \mathbf{0} & \Sigma \end{array}\right]\boldsymbol{\zeta} + \begin{bmatrix} \boldsymbol{B}_2(e_{y_2})p(e_{y_2}) \\ \boldsymbol{B}_1(e_{z_2})f(e_{z_2}) \\ \mathbf{0} \end{bmatrix} \tag{43b}$$

By splitting u_c in the constant desired velocity U_{rd} and the adaptive part $g(x)$ the coupling between the coordination dynamics and path-following error dynamics becomes evident

$$\dot{\boldsymbol{\phi}} = \boldsymbol{f}(\boldsymbol{\phi}) + \boldsymbol{G}(\boldsymbol{\zeta}, \boldsymbol{\phi})\boldsymbol{\zeta} \tag{44a}$$

$$\begin{aligned}\dot{\boldsymbol{\zeta}} = &\left[\begin{array}{c|cc} \boldsymbol{A}_2(e_{y_2}, U_{rd}) & \multicolumn{2}{c}{\boldsymbol{H}_2} \\ \hline \mathbf{0} & \boldsymbol{A}_1(e_{z_2}, U_{rd}) & \boldsymbol{H}_1 \\ & \mathbf{0} & \Sigma \end{array}\right]\boldsymbol{\zeta} \\ &+ \begin{bmatrix} \boldsymbol{B}_2(e_{y_2})p(e_{y_2}) \\ \boldsymbol{B}_1(e_{z_2})f(e_{z_2}) \\ \mathbf{0} \end{bmatrix} + \begin{bmatrix} \boldsymbol{C}_2(e_{y_2}) \\ \boldsymbol{C}_1(e_{z_2}) \\ \mathbf{0} \end{bmatrix} g(x)\end{aligned} \tag{44b}$$

where $\boldsymbol{C}g(x)$ is the feedback from coordination dynamics in path-following dynamics.

$$\boldsymbol{A}_1 \triangleq \begin{bmatrix} \frac{-\sigma_z\Delta_z}{(e_{z_2}+\sigma_z z_{\text{int}}^{\text{eq}})^2+\Delta_z^2} & \frac{\Delta_z}{(e_{z_2}+\sigma_z z_{\text{int}}^{\text{eq}})^2+\Delta_z^2} & 0 \\ \frac{-\sigma_z^2\Delta_z}{(e_{z_2}+\sigma_z z_{\text{int}}^{\text{eq}})^2+\Delta_z^2} & \left(\frac{\sigma_z\Delta_z}{(e_{z_2}+\sigma_z z_{\text{int}}^{\text{eq}})^2+\Delta_z^2}-\frac{u_c}{\sqrt{(e_{z_2}+\sigma_z z_{\text{int}}^{\text{eq}})^2+\Delta_z^2}}\right) & \frac{\Delta_z}{\sqrt{(e_{z_2}+\sigma_z z_{\text{int}}^{\text{eq}})^2+\Delta_z^2}} \\ \frac{-\sigma_z^2\Delta_z^2 X_{wr}^{u_c}}{((e_{z_2}+\sigma_z z_{\text{int}}^{\text{eq}})^2+\Delta_z^2)^2} & \left(\frac{\sigma_z\Delta_z^2 X_{wr}^{u_c}}{((e_{z_2}+\sigma_z z_{\text{int}}^{\text{eq}})^2+\Delta_z^2)^2}+\frac{Z_{w_r}}{\sqrt{(e_{z_2}+\sigma_z z_{\text{int}}^{\text{eq}})^2+\Delta_z^2}}-\frac{u_c\Delta_z X_{wr}^{u_c}}{((e_{z_2}+\sigma_z z_{\text{int}}^{\text{eq}})^2+\Delta_z^2)^{3/2}}\right) & \left(Y_{wr}^{u_c}-\frac{\Delta_z^2 X_{wr}^{u_c}}{((e_{z_2}+\sigma_z z_{\text{int}}^{\text{eq}})^2+\Delta_z^2)^{3/2}}\right) \end{bmatrix} \tag{29}$$

$$\boldsymbol{A}_2 \triangleq \begin{bmatrix} -\frac{\sigma_y\Delta_y}{(e_{y_2}+\sigma_y y_{\text{int}}^{\text{eq}})^2+\Delta_y^2} & \frac{\Delta_y}{(e_{y_2}+\sigma_y y_{\text{int}}^{\text{eq}})^2+\Delta_y^2} & 0 \\ -\frac{\sigma_y^2\Delta_y}{(e_{y_2}+\sigma_y y_{\text{int}}^{\text{eq}})^2+\Delta_y^2} & \left(\frac{\sigma_y\Delta_y}{(e_{y_2}+\sigma_y y_{\text{int}}^{\text{eq}})^2+\Delta_y^2}-\frac{\Gamma(s)}{\sqrt{(e_{y_2}+\sigma_y y_{\text{int}}^{\text{eq}})^2+\Delta_y^2}}\right) & \frac{\Delta_y}{\sqrt{(e_{y_2}+\sigma_y y_{\text{int}}^{\text{eq}})^2+\Delta_y^2}} \\ \frac{1}{\sqrt{s^2+1}}\frac{\sigma_y^2\Delta_y^2 X_{wr}^{u_c}}{((e_{y_2}+\sigma_y y_{\text{int}}^{\text{eq}})^2+\Delta_y^2)^2} & \frac{1}{\sqrt{s^2+1}}\left(\frac{\Gamma(s)\Delta_y X_{wr}^{u_c}}{((e_{y_2}+\sigma_y y_{\text{int}}^{\text{eq}})^2+\Delta_y^2)^{3/2}}-\frac{\sigma_y\Delta_y^2 X_{wr}^{u_c}}{((e_{y_2}+\sigma_y y_{\text{int}}^{\text{eq}})^2+\Delta_y^2)^2}\right) & \left(Y_{wr}^{u_c}-\frac{\Delta_y^2 X_{wr}^{u_c}}{\sqrt{s^2+1}((e_{y_2}+\sigma_y y_{\text{int}}^{\text{eq}})^2+\Delta_y^2)^{3/2}}\right) \end{bmatrix} \tag{30}$$

V. Closed-loop Stability

Note that the coupling term seen in (44b) is a result of the combination of having a multi-agent system and having disturbance rejection. With only one of these, the system would be in a cascaded form. Now instead the system has a feedback-interconnected form. However, feedback-interconnected systems can be analysed as cascade-interconnected system using a technique called 'breaking the loop', as introduced in [1]. In [1] it is shown how a system of the form:

$$\dot{x}_1 = f_1(t, x_1) + g(t, x_1, x_2) \tag{45a}$$
$$\dot{x}_2 = f_2(t, x_1, x_2) \tag{45b}$$

can be analysed as a cascaded system of the form

$$\dot{\xi}_1 = f_1(t, \xi_1) + g(t, \xi_1, \xi_2)\xi_2 \tag{46a}$$
$$\dot{\xi}_2 = f_2(t, x_1(t), \xi_2) = \tilde{f}_2(t, \xi_2) \tag{46b}$$

where $f_2(t, x_1(t), \xi_2)$ depends on the *parameter* x_1, with $x_1(t)$ denoting solutions of (45a), under the conditions that

1) $x_1 = 0$ is a UGAS equilibrium for $\dot{x}_1 = f_1(t, x_1)$.
2) The solutions of (45) are uniformly globally bounded.

Condition 1) translates to the closed-loop system (43) satisfying the following condition:

Condition 1: $\boldsymbol{\phi} = 0$ is a UGAS equilibrium for $\dot{\boldsymbol{\phi}} = \boldsymbol{f}(\boldsymbol{\phi})$.

Condition 1 is verified by claim 3) from Lemma 1.

Verifying condition 2) requires satisfying the following subconditions

Condition 2a: There exists a $\mathcal{C}^1$ positive definite radially unbounded function $\tilde{V} : \mathbb{R} \times \mathbb{R}^{n_1} \to \mathbb{R}_{\geq 0}, \alpha_1 \in \mathcal{K}_\infty$ and continuous non-decreasing functions $\alpha_4, \alpha_4' : \mathbb{R}_{\geq 0} \times \mathbb{R} \to \mathbb{R}_{\geq 0}$ such that

$$\tilde{V}(t, x_1) \geq \alpha_1(|x_1|) \tag{47}$$
$$\dot{\tilde{V}}_{(43a)}(t, x_1) \leq \alpha_4(|x_1|)\alpha_4'(|x_2|); \tag{48}$$
$$\int_a^\infty \frac{\mathrm{d}\tilde{v}}{\alpha_4(\alpha_1^{-1}(\tilde{v}))} = \infty \tag{49}$$

Condition 2a can be verified using the function

$$\tilde{V}_{(43a)}(\boldsymbol{\phi}) = \tfrac{1}{2}\boldsymbol{\phi}^2 \tag{50}$$

which is clearly $\mathcal{K}_\infty$, satisfying (47). From (50) it follows that

$$\dot{\tilde{V}}_{(43a)}(\boldsymbol{\phi}) \triangleq \frac{\partial \tilde{V}}{\partial t} + \frac{\partial \tilde{V}}{\partial \boldsymbol{\phi}}[\boldsymbol{f}(\boldsymbol{\phi}) + \boldsymbol{G}(\boldsymbol{\zeta}, \boldsymbol{\phi})\boldsymbol{\zeta}] = \boldsymbol{\phi}^T\dot{\boldsymbol{\phi}}. \tag{51}$$

Using (41) and (32) it can be verified that functions

$$\alpha_4(|\boldsymbol{\phi}|) \triangleq |\boldsymbol{\phi}|^T \tag{52}$$
$$\alpha_4'(|\boldsymbol{\zeta}|) \triangleq |\boldsymbol{T}| \begin{bmatrix} 5a+|\tilde{u}_{r_1}|+|v_{r_1}|+|e_{z_{31}}|+3|w_{r_1}^{\text{eq}}|+3|U_{rd_1}| \\ \vdots \\ 5a+|\tilde{u}_{r_n}|+|v_{r_n}|+|e_{z_{3n}}|+3|w_{r_n}^{\text{eq}}|+3|U_{rd_n}| \end{bmatrix} \tag{53}$$

satisfy the inequality

$$\dot{\tilde{V}}_{(43a)}(\boldsymbol{\phi}) \leq \alpha_4(|\boldsymbol{\phi}|)\alpha_4'(|\boldsymbol{\zeta}|)$$

with $\alpha_4, \alpha_4' : \mathbb{R}_{\geq 0} \times \mathbb{R} \to \mathbb{R}_{\geq 0}$ continuous and non-decreasing w.r.t. their arguments.

To verify that (49) holds, note that $\alpha_1^{-1}(\tilde{v}) = \sqrt{2\tilde{v}}$ and consequently it holds that

$$\int_a^\infty \frac{\mathrm{d}\tilde{v}}{\alpha_4(\alpha_1^{-1}(\tilde{v}))} = \int_a^\infty \frac{\mathrm{d}\tilde{v}}{\sqrt{2\tilde{v}}} = \infty.$$

Condition 2b: We dispose of a $\mathcal{C}^1$ function $V : \mathbb{R}\times\mathbb{R}^{n_1} \to \mathbb{R}_{\geq 0}$, $\alpha_1, \alpha_2 \in \mathcal{K}_\infty$, and a positive semidefinite function W such that

$$\alpha_1(|x_1|) \leq V(t, x_1) \leq \alpha_2(|x_1|) \tag{54}$$
$$\frac{\partial V}{\partial t} + \frac{\partial V}{\partial x_1} f_1(t, x_1) \leq -W(x_1) \tag{55}$$

for all $t \in [t_o, t_{\max})$ and all $x_1 \in \mathbb{R}^{n_1}$.

Condition 2b holds as a direct consequence of Condition 1 being satisfied.

Condition 2c: There exists $\beta \in \mathcal{KL}$ such that the solutions $x_2(t, t_o, x_{2o}, x_1)$ of $\dot{x}_2 = \tilde{f}_2(t, x_2)$ satisfy

$$|x_2(t, t_o, x_{2o}, x_1)| \leq \beta(|x_{2o}|, t - t_o) \quad \forall t \in [t_o, t_{\max}). \tag{56}$$

To show that Condition 2c holds the stability proof of the path-following strategy from [17] is utilised. It should be noted that $|x_2(t, t_o, x_{2o}, x_1)|$ represents the solutions of (45b) for fixed values of the parameter x_1, i.e. solutions of the path-following error dynamics (44b) for fixed values of the coordination error $\boldsymbol{\phi}$ and hence fixed values of the velocity. Consequently, the stability proof from [17] for UGAS and ULES of the origin of (44b) implies that inequality (56) holds. However UGAS of the origin of (44b) cannot be claimed since (56) only holds for the existence of the solutions [1].

Condition 2) is now verified with the following theorem:

Theorem 2: Consider system (43) under the following conditions:

$$\alpha_5(|\boldsymbol{\phi}|) \triangleq C_1 \tag{57}$$
$$\alpha_5'(|\boldsymbol{\zeta}|) \triangleq \alpha_4'(|\boldsymbol{\zeta}|) \tag{58}$$

with C_1 from (38). Then, the solutions of (43) are uniformly globally bounded.

Proof: Theorem 2 holds, since using (58) and (57) it can be verified that [1, Theorem 2], which is given as Theorem A.1 in Appendix II, holds for system (43). ■

Theorem 3: The origin of (43) is UGAS if Condition 1 and the conditions of Theorem 2 hold.

Proof: It is shown that both Condition 1 and Theorem 2 hold and hence we can invoke [1, Proposition 2], given as Proposition A.1 in Appendix II, for system (43). ■

TABLE I
SIMULATION PARAMETERS.

Variable	Value	Unit	Variable	Value	Unit
Δ_y	10	m	σ_y, σ_z	0.2	-
Δ_z	20	m	d_{12}, d_{13}	50	m
V_x	-0.11028	m/s	V_y	0.08854	m/s
V_z	-0.05	m/s	D_{z_1}	-20	m
D_{z_2}, D_{z_3}	-10	m	D_{y_1}	0	m
D_{y_2}	-50	m	D_{y_3}	50	m
U_{rd}	2	m/s	a	0.2	m/s

This implies that the control goals (6) are achieved and thus the proof of Theorem 1 is complete. The results are illustrated with a case study in the next section.

VI. CASE STUDY

This case study considers three AUVs moving in three dimensional space affected by a constant three dimensional ocean current. The parameters for the model (2) are obtained from [23]. The simulation parameters to describe the formation, the ocean current, the tuning of the integral line-of-sight guidance, and the formation control strategy are given in Table I. It can be verified that these parameters satisfy all conditions of Theorem 1. The initial position for the AUVs is given by

$$\begin{bmatrix} x_{1o} \\ y_{1o} \\ z_{1o} \\ \theta_{1o} \\ \psi_{1o} \end{bmatrix} = \begin{bmatrix} 0 \\ -100 \\ -50 \\ 0 \\ \pi \end{bmatrix}, \quad \begin{bmatrix} x_{2o} \\ y_{2o} \\ z_{2o} \\ \theta_{2o} \\ \psi_{2o} \end{bmatrix} = \begin{bmatrix} 0 \\ 50 \\ -50 \\ 0 \\ \pi/2 \end{bmatrix}, \quad \begin{bmatrix} x_{3o} \\ y_{3o} \\ z_{3o} \\ \theta_{3o} \\ \psi_{3o} \end{bmatrix} = \begin{bmatrix} 0 \\ -50 \\ -50 \\ 0 \\ -\pi/2 \end{bmatrix}.$$

The communication topology is as follows: AUV-1 communicates it position to both AUV-2 and AUV-3, and AUV-3 communicates its position to AUV-1. Note that this makes AUV-1 a globally reachable vertex in the Laplacion of the communication graph. Hence, the conditions in Subsection II-C and Section IV are satisfied.

The motion of the vehicles in three dimensional space can be seen in Figure 2. From Figure 2 it can be seen that the vehicles converge to their assigned path. This is confirmed by the error plots in Figure 3. From which is it can be seen that the y- and z-direction path-following errors converge to zero. Figure 4 shows that the along-path formation errors go to zero and the desired formation is achieved. The actuation signals required by the control strategy can be seen in Figure 5.

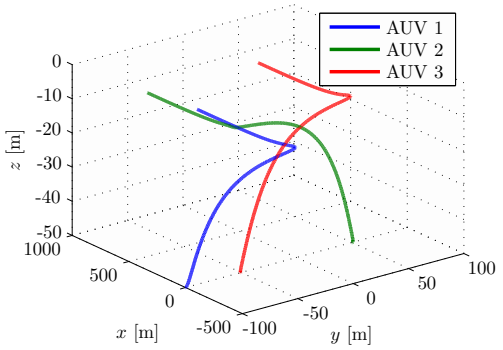

Fig. 2. AUV trajectories in 3-D space

VII. CONCLUSIONS

In this paper a control strategy for straight-line coordinated path-following of under-actuated vehicles moving in three dimensional space has been presented. It has been shown that using integral LOS guidance the vehicles are able to reject an unknown, but constant, environmental disturbance, whilst simultaneously coordinating their

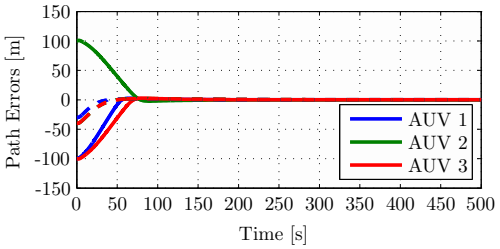

Fig. 3. Path following errors y (solid) and z (dashed)

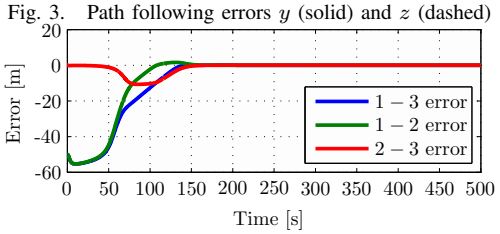

Fig. 4. Along-path formation errors

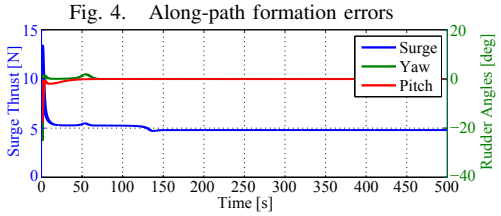

Fig. 5. Actuation signals

motion along a desired path with a nonlinear decentralised coordination law to achieve a desired formation. The origin of the combined coordination and path-following error dynamics is shown to be UGAS by showing that our feedback-interconnected system can be analysed as a cascaded system and satisfies the conditions to prove UGAS. Simulation results were presented that validate the theoretical results.

APPENDIX I
FUNCTION DEFINITIONS

$$\begin{aligned}
F_{u_r}(v_r, w_r, r, q) &\triangleq \tfrac{1}{m_{11}}[(m_{22}v_r + m_{25}r)r - (m_{33}w_r + m_{34}q)q], \\
X_{v_r}(u_r) &\triangleq \tfrac{m_{25}^2 - m_{11}m_{55}}{m_{22}m_{55} - m_{25}^2}u_r + \tfrac{d_{55}m_{25} - d_{25}m_{55}}{m_{22}m_{55} - m_{25}^2}, \\
Y_{v_r}(u_r) &\triangleq \tfrac{(m_{22} - m_{11})m_{25}}{m_{22}m_{55} - m_{25}^2}u_r - \tfrac{d_{22}m_{55} - d_{52}m_{25}}{m_{22}m_{55} - m_{25}^2}, \\
X_{w_r}(u_r) &\triangleq \tfrac{-m_{34}^2 + m_{11}m_{44}}{m_{33}m_{44} - m_{34}^2}u_r + \tfrac{d_{44}m_{34} - d_{34}m_{44}}{m_{33}m_{44} - m_{34}^2}, \\
Y_{w_r}(u_r) &\triangleq \tfrac{(m_{11} - m_{33})m_{34}}{m_{33}m_{44} - m_{34}^2}u_r - \tfrac{d_{33}m_{44} - d_{43}m_{34}}{m_{33}m_{44} - m_{34}^2}, \\
Z_{w_r} &\triangleq \tfrac{BG_z W m_{34}}{m_{33}m_{44} - m_{34}^2}, \\
F_q(\theta, u_r, w_r, q) &\triangleq \tfrac{m_{34}d_{33} - m_{33}(d_{43} - (m_{33} - m_{11})u_r)}{m_{33}m_{44} - m_{34}^2}w_r \\
&\quad + \tfrac{m_{34}(d_{34} - m_{11}u_r) - m_{33}(d_{44} - m_{34}u_r)}{m_{33}m_{44} - m_{34}^2}q \\
&\quad - \tfrac{BG_z W m_{33}}{m_{33}m_{44} - m_{34}^2}\sin(\theta), \\
F_r(u_r, v_r, r) &\triangleq \tfrac{m_{25}d_{22} - m_{22}(d_{53} + (m_{22} - m_{11})u_r)}{m_{22}m_{55} - m_{25}^2}v_r \\
&\quad + \tfrac{m_{25}(d_{25} + m_{11}u_r) - m_{22}(d_{55} + m_{25}u_r)}{m_{22}m_{55} - m_{25}^2}r.
\end{aligned}$$

Vectors $\boldsymbol{h}_z \triangleq [h_{z1}, h_{z2}, h_{z3}, h_{z4}, h_{z5}]^T$ and $\boldsymbol{h}_{w_r} \triangleq [h_{w_r1}, h_{w_r2}, h_{w_r3}, h_{w_r4}, h_{w_r5}]^T$ are defined as:

$$\begin{aligned}
h_{z1} &= -\sin(\tilde{\theta} + \theta_d); \quad h_{z2} = h_{z3} = h_{z5} = 0 \\
h_{z4} &= w_r\left[\tfrac{\cos(\tilde{\theta}) - 1}{\tilde{\theta}}\cos(\theta_d) - \tfrac{\sin(\tilde{\theta})}{\tilde{\theta}}\sin(\theta_d)\right] \\
&\quad - u_c\left[\tfrac{\sin(\tilde{\theta})}{\tilde{\theta}}\cos(\theta_d) + \tfrac{\cos(\tilde{\theta}) - 1}{\tilde{\theta}}\sin(\theta_d)\right] \\
h_{w_r1} &= \tfrac{X_{w_r}(\tilde{u}_r + u_c) - X_{w_r}^{u_c}}{\tilde{u}_r}\gamma_{w_r}(z_{\text{int}}, z, w_r) \\
&\quad + w_r\tfrac{Y_{w_r}(\tilde{u}_r + u_c) - Y_{w_r}^{u_c}}{\tilde{u}_r},
\end{aligned}$$

$$h_{w_r4} = Z_{w_r}\left[\frac{\sin(\tilde{\theta})}{\tilde{\theta}}\cos(\theta_d) + \frac{\cos(\tilde{\theta}-1)}{\tilde{\theta}}\sin(\theta_d)\right],$$
$$h_{w_r5} = X_{w_r}(\tilde{u}_r + u_c); \quad h_{w_r2} = h_{w_r3} = 0.$$

The vectors $\boldsymbol{h}_y \triangleq [h_{y1}, h_{y2}, h_{y3}, h_{y4}, h_{y5}, h_{y6}, h_{y7}, h_{y8}]^T$ and $\boldsymbol{h}_{v_r} \triangleq [h_{v_r1}, h_{v_r2}, h_{v_r3}, h_{v_r4}, h_{v_r5}, h_{v_r6}, h_{v_r7}, h_{v_r8}]^T$ are defined as:

$$h_{y2} = \frac{u_c}{e_{z2}}\left[\frac{\Delta_z}{\sqrt{(e_{z_2}+\sigma_z z_{\text{int}}^{\text{eq}})^2+\Delta_z^2}} - \frac{1}{\sqrt{s^2+1}}\right]$$
$$- \frac{s}{\sqrt{s^2+1}}\frac{Z_{w_r}}{Y_{w_r}^{u_c}}\frac{1}{e_z}\left[\frac{e_{z_2}+\sigma_z z_{\text{int}}^{\text{eq}}}{\sqrt{(e_{z_2}+\sigma_z z_{\text{int}}^{\text{eq}})^2+\Delta_z^2}} - \frac{s}{\sqrt{s^2+1}}\right],$$
$$h_{y3} = \sin(\tilde{\theta}+\theta_d)\sin(\tilde{\psi}+\psi_d),\ h_{y4} = \cos(\tilde{\theta}+\theta_d)\sin(\tilde{\psi}+\psi_d)$$
$$h_{y5} = \left[u_c\cos(\tilde{\theta}+\theta_d) - \frac{s}{\sqrt{s^2+1}}\frac{Z_{w_r}}{Y_{w_r}^{u_c}}\sin(\tilde{\theta}+\theta_d)\right]$$
$$\cdot\left[\frac{\sin(\tilde{\psi})}{\tilde{\psi}}\cos(\psi_d) + \frac{\cos(\tilde{\psi}-1)}{\tilde{\psi}}\sin(\psi_d)\right]$$
$$+ v_r\left[\frac{\cos(\tilde{\psi})-1}{\tilde{\psi}}\cos(\psi_d) - \frac{\sin(\tilde{\psi})}{\tilde{\psi}}\sin(\psi_d)\right],$$
$$h_{y7} = u_c\sin(\psi_d)\left[\frac{\cos(\tilde{\theta})-1}{\tilde{\theta}}\cos(\theta_d) - \frac{\sin(\tilde{\theta})}{\tilde{\theta}}\sin(\theta_d)\right]$$
$$- \frac{s}{\sqrt{s^2+1}}\frac{Z_{w_r}}{Y_{w_r}^{u_c}}\sin(\psi_d)\left[\frac{\sin(\tilde{\theta})}{\tilde{\theta}}\cos(\theta_d) + \frac{\cos(\tilde{\theta})-1}{\tilde{\theta}}\sin(\theta_d)\right]$$
$$h_{y1} = h_{y6} = h_{y8} = 0,$$
$$h_{v_r2} = \frac{X_{v_r}^{u_c}}{e_{z_2}}\left[\frac{\Delta_z}{\sqrt{(e_{z_2}+\sigma_z z_{\text{int}}^{\text{eq}})^2+\Delta_z^2}} - \frac{1}{\sqrt{s^2+1}}\right]\gamma_{v_r}(y_{\text{int}}, y, v_r),$$
$$h_{v_r4} = \frac{X_{v_r}(\tilde{u}_r+u_c) - X_{v_r}^{u_c}}{\tilde{u}_r}\cos(\tilde{\theta}+\theta_d)\gamma_{v_r}(y_{\text{int}}, y, v_r)$$
$$+ v_r\frac{Y_{v_r}(\tilde{u}_r+u_c) - Y_{v_r}^{u_c}}{\tilde{u}_r},$$
$$h_{v_r6} = X_{v_r}(\tilde{u}_r+u_c)\cos(\tilde{\theta}+\theta_d),\ h_{v_r1} = h_{v_r3} = h_{v_r5} = h_{v_r8} = 0$$
$$h_{v_r7} = \left[\frac{\cos(\tilde{\theta})-1}{\tilde{\theta}}\cos(\theta_d) - \frac{\sin(\tilde{\theta})}{\tilde{\theta}}\sin(\theta_d)\right]X_{v_r}^{u_c}\gamma_{v_r}(y_{\text{int}}, y, v_r).$$

Functions $\gamma_{w_r}(z_{\text{int}}, z, w_r)$ and $\gamma_{v_r}(y_{\text{int}}, y, v_r)$ are defined as

$$\gamma_{w_r} \triangleq \frac{\Delta_z u_c(z+\sigma_z z_{\text{int}})}{((z+\sigma_z z_{\text{int}}^{\text{eq}})^2+\Delta_z^2)^{3/2}} + \frac{\Delta_z^2}{((z+\sigma_z z_{\text{int}}^{\text{eq}})^2+\Delta_z^2)^{3/2}}w_r$$
$$+ \frac{\sigma_z\Delta_z^2}{((z+\sigma_z z_{\text{int}}^{\text{eq}})^2+\Delta_z^2)^2}z + \frac{\Delta_z V_z}{(z+\sigma_z z_{\text{int}}^{\text{eq}})^2+\Delta_z^2)},$$
$$\gamma_{v_r} \triangleq \frac{\Delta_y\Gamma(s)(y+\sigma_y y_{\text{int}}}{((y+\sigma_y y_{\text{int}}^{\text{eq}})^2+\Delta_y^2)^{3/2}} - \frac{\Delta_y^2}{((y+\sigma_y y_{\text{int}}^{\text{eq}})^2+\Delta_y^2)^{3/2}}v_r$$
$$- \frac{\sigma_y\Delta_y^2}{((y+\sigma_y y_{\text{int}}^{\text{eq}})^2+\Delta_y^2)^2}y - \frac{\Delta_y V_y}{(y+\sigma_y y_{\text{int}}^{\text{eq}})^2+\Delta_y^2)}.$$

APPENDIX II
REFERENCE THEOREMS

This appendix presents Theorem 2 and Proposition 2 from [1] which are used in the stability proof of the closed-loop system in Section V.

Theorem A.1 ([1, Theorem 2]): Consider system (45) under the following conditions:

1) Condition 2a, 2b, and 2c hold;
2) there exist α_5, $\alpha_5' \in \mathcal{K}$ such that

$$|[L_g V]| \leq \alpha_5(|x_1|)\alpha_5'(|x_2|) \tag{59}$$

and for each $r > 0$ there exist λ_r, $\eta_r > 0$ such that

$$t \geq 0,\ |x_1| \geq \eta_r \implies \alpha_5(|x_1|) \leq \lambda_r W(x_1) \tag{60}$$

Then, the solutions of (45) are uniformly globally bounded.

Proposition A.1 ([1, Proposition 2]): Under Condition 1 and the conditions of Theorem 2 the origin of (45) is UGAS.

REFERENCES

[1] A. Loría, "From feedback to cascade-interconnected systems: Breaking the loop," in *Decision and Control, 2008. CDC 2008. 47th IEEE Conference on*. IEEE, 2008, pp. 4109–4114.

[2] H. Bai, M. Arcak, and J. T. Wen, *Cooperative control design*. Springer, 2011, vol. 89.

[3] V. Kumar, N. Leonard, and A. Morse, *Cooperative Control*. Springer-Verlag, 2005.

[4] K. Y. Pettersen, J. T. Gravdahl, and H. Nijmeijer, *Group coordination and cooperative control*. Springer Berlin, 2006, vol. 336.

[5] A. Jadbabaie, J. Lin, and A. S. Morse, "Coordination of groups of mobile autonomous agents using nearest neighbor rules," *IEEE Transactions on Automatic Control*, vol. 48, no. 6, pp. 988–1001, 2003.

[6] R. W. Beard, J. Lawton, and F. Y. Hadaegh, "A coordination architecture for spacecraft formation control," *IEEE Transactions on control systems technology*, vol. 9, no. 6, pp. 777–790, 2001.

[7] I. Kaminer, O. Yakimenko, A. Pascoal, and R. Ghabcheloo, "Path generation, path following and coordinated control for timecritical missions of multiple uavs," in *American Control Conference, 2006*. IEEE, 2006, pp. 4906–4913.

[8] D. M. Stipanović, G. Inalhan, R. Teo, and C. J. Tomlin, "Decentralized overlapping control of a formation of unmanned aerial vehicles," *Automatica*, vol. 40, no. 8, pp. 1285–1296, 2004.

[9] K. D. Do and J. Pan, "Nonlinear formation control of unicycle-type mobile robots," *Robotics and Autonomous Systems*, vol. 55, no. 3, pp. 191–204, 2007.

[10] J. Dasdemir and A. Loria, "Robust formation-tracking control of mobile robots via one-to-one time-varying communication," *International Journal of Control*, pp. 1–17, 2014.

[11] R. Ghabcheloo, A. P. Aguiar, A. Pascoal, C. Silvestre, I. Kaminer, and J. Hespanha, "Coordinated path-following in the presence of communication losses and time delays," *SIAM Journal on Control and Optimization*, vol. 48, no. 1, pp. 234–265, 2009.

[12] L. Lapierre, D. Soetanto, and A. Pascoal, "Nonlinear path following with applications to the control of autonomous underwater vehicles," in *Proc. of the 42nd IEEE Conference on Decision and Control*, vol. 2, 2003, pp. 1256–1261.

[13] E. Børhaug, A. Pavlov, E. Panteley, and K. Y. Pettersen, "Straight line path following for formations of underactuated marine surface vehicles," *IEEE Transactions on Control Systems Technology*, vol. 19, no. 3, pp. 493–506, 2011.

[14] D. J. W. Belleter and K. Y. Pettersen, "Path following for formations of underactuated marine vessels under influence of constant ocean currents," in *Proceedings of the 53th IEEE Conference on Decision and Control, Los Angeles, USA, Dec. 15-17*, 2014, pp. 4521–4528.

[15] ——, "Path following with disturbance rejection for inhomogeneous formations with underactuated agents," in *European Control Conference, Linz, Austria*, 2015.

[16] W. Caharija, K. Y. Pettersen, J. T. Gravdahl, and E. Børhaug, "Path following of underactuated autonomous underwater vehicles in the presence of ocean currents," in *Proc. of the 51th IEEE Conference on Decision and Control*, 2012, pp. 528–535.

[17] W. Caharija, K. Y. Pettersen, M. Bibuli, P. Calado, E. Zereik, J. Braga, J. T. Gravdahl, A. J. Sørensen, M. Milovanović, and G. Bruzzone, "Integral line-of-sight guidance and control of underactuated marine vehicles," *Submitted to: IEEE Transactions on Control Systems Technology*, 2015.

[18] T. I. Fossen, *Handbook of Marine Craft Hydrodynamics and Motion Control*. Wiley, 2011.

[19] E. Børhaug, A. Pavlov, and K. Y. Pettersen, "Straight line path following for formations of underactuated underwater vehicles," in *Proc. of the 46th IEEE Conference on Decision and Control*, 2007, pp. 2905–2912.

[20] M. Mesbahi and M. Egerstedt, *Graph theoretic methods in multiagent networks*. Princeton University Press, 2010.

[21] C. Godcil and G. Royle, "Algebraic graph theory," *Ser. Springer Graduate Texts in Mathematics*, vol. 207, 2001.

[22] E. Børhaug, A. Pavlov, and K. Y. Pettersen, "Integral los control for path following of underactuated marine surface vessels in the presence of ocean currents," in *Proc. of the 47th IEEE Conference on Decision and Control*, 2008, pp. 4984–4991.

[23] J. E. da Silva, B. Terra, R. Martins, and J. B. de Sousa, "Modeling and simulation of the lauv autonomous underwater vehicle," in *13th IEEE IFAC International Conference on Methods and Models in Automation and Robotics*, 2007.